Journal of Materials and Environmental Sciences
ISSN : 2028-2508
CODEN : JMESCN

J. Mater. Environ. Sci., 2018, Volume 9, Issue 6, Page 1796-1808

https://doi.org/10.26872/jmes.2018.9.6.200

http://www.jmaterenvironsci.com

Adsorption Properties and Inhibition of Carbon Steel Corrosion in Hydrochloric Acid Solution by Novel Diazepine Derivatives: Experimental and Theoretical Studies

T. Laabaissi[1], M. Rbaa[2], K. Ourrak[3], H. Zarrok[1*], M. El Faydy[2], B. Lakhrissi[2], H. Lgaz[1], R. Touir[4,5], I. Warad[6], H. Oudda[1*]

1. *Laboratoire des procèdes de séparation, Faculté des Sciences, Université Ibn Tofail, Kenitra, BP 133, Kenitra, Morocco*
2. *Laboratoire d'Agro ressources et Génie des Procédés, Université Ibn Tofail, Faculté des Sciences, Département de Chimie, B.P. 133, Kénitra, Morocco.*
3. *Laboratory of Chemistry/Biology Applied to the Environment, Faculty of Sciences, Moulay Ismail University, BP 11201-ZItoune, Meknès, 50070, Morocco.*
4. *Laboratoire d'Ingénierie des Matériaux et d'Environnement : Modélisation et Application, Faculté des Sciences, Université Ibn Tofail, BP 133, Kénitra 14 000, Morocco.*
5. *Centre Régional des Métiers de l'Education et de la Formation (CRMEF), Avenue Allal Al Fassi, Madinat Al Irfane BP 6210 Rabat, Morocco.*
6. *Department of Chemistry, AN-Najah National University P.O. Box 7, Nablus, Palestine.*

Received 18 Jul 2017,
Revised 12 Jan 2018,
Accepted 18 Jan 2018

Keywords

- ✓ Acidic medium;
- ✓ Benzodiazepine derivatives;
- ✓ Corrosion inhibition;
- ✓ Monte Carlo simulations

H. Oudda
ouddahassan@gmail.com

Abstract

Two benzodiazepine derivatives namely, 2,2,4,8-tetramethyl-2,3-dihydro-1H-benzo[b][1,4]diazepine (THBD), 8-chloro-2,2,4-trimethyl-2,3-dihydro-1H-benzo[b][1,4] diazepine (CTHBD) were examined as a corrosion inhibitor for carbon steel in 1.0 M HCl using electrochemical impedance spectroscopy (EIS) and potentiodunamic polarization (PP). The results showed that both compounds are good inhibitors and their inhibition efficiencies increase with their concentrations to reache 92 % at 5×10^{-3} M. The Tafel polarization study revealed that both inhibitors act as a mixed type inhibitors. Furthermore, it has been established that their adsorption follow the Langmuir adsorption isotherm. In addition, the thermodynamic activation parameters for the corrosion reaction were calculated and discussed in relation to the stability of the protective layer. Finally, quantum chemical parameters were calculated using the Density Functional Theory method (DFT) and Monte Carlo simulations. It is found that the correlation between theoretical and experimental results was discussed.

1. Introduction

Carbon steel is among the most widely used engineering materials in different applications [1–10]. Acid solutions are widely used in industries for pickling, acid cleaning of boilers, decaling and oil well acidizing. Mostly, sulfuric and hydrochloric acids are employed for such purposes. In these medium, the main problem concerning carbon steel applications is its relatively low corrosion resistance [11–19]. Several methods are currently used to prevent the above cited problems. One such method is the use of an organic inhibitor [20–25]. In research on organic corrosion inhibitors, attention is paid to the mechanism of adsorption and also to the relationship between inhibitor structures and their adsorption properties. It has been observed that the adsorption depends mainly on the electronic and structural properties of the inhibitor molecule such as functional groups, steric factors, aromaticity, electron density on donor atoms and π-orbital character of donating electrons. Density functional theory (DFT) for instance, has been used to predict the molecular geometry, electronic properties and active sites of organic corrosion inhibitors [26]. This could help in the understanding of specific sites of interaction between the inhibitor and the metal surface. On the other hand, Monte Carlo simulation can provide us useful information about the low energy adsorption configuration of an organic inhibitor onto a metal surface which cannot be evaluated experimentally [21].

This work is devoted to study the inhibition characteristics of two synthesized benzodiazepine derivatives for carbon steel in 1.0 M HCl, using potentiodynamic polarization measurements and electrochemical impedance spectroscopy coupled with DFT method and Monte Carlo simulation.

2. Experimental details

2.1. Synthesis of inhibitors

General Procedure

An equimolar amount of substituted orthophenylene (1a, b) is mixed with absolute acetone in absolute ethanol at reflux under magnetic stirring for 24 hours after characterization of the reaction by TLC (thin tail chromatography). The treatment of the reaction consists in bringing the mixture to a temperature of room temperature, after 1 hour a solid has appeared, this solid is filtered, washed with distilled water, dried in an oven and recrystallized in absolute ethanol. In this synthesis, we adopted the method of Shi et al. [27], schema1

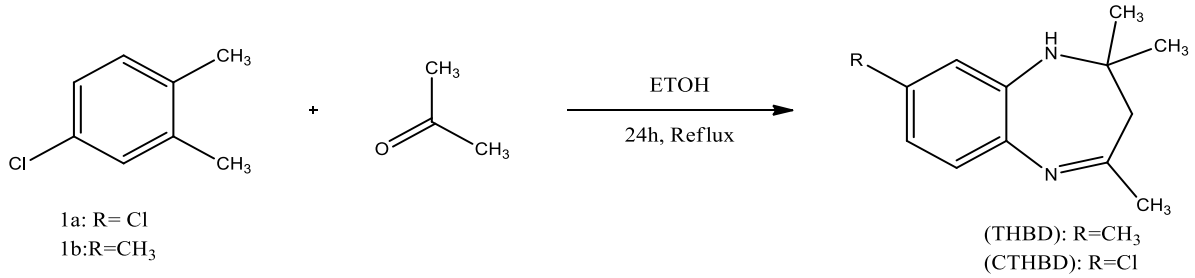

Scheme 1: synthesis of benzodiazepines derivatives THBD and CTHBD

So, the 8-chloro-2,2,4-trimethyl-2,3-dihydro-1H-benzo[b][1,4]diazepine [CTHBD] was synthesized from 4-chloro-ortho-phenylene and 2,2,4,8-tetramethyl-2,3-dihydro-1H-benzo[b][1,4]diazepine [THBD] from 4-methyl-orthophenylenediamine with acetone according to the general procedure. Their characteristics were presented in Table 1.

Table 1: IR and characterization of the synthesis compounds

Compounds	Number of waves (cm^{-1})	Functional Grouping	Yield %	R_f	Appearance
CTHBD	800-600	C-Cl	70	0.80	Yellow solid
	1635	C=N			
	1300-1600	C=C			
	3100-3500	NH			
THBD	1633	C=N	50	0.9	Yellow solid
	3310-3500	NH			
	1450-1500	C=C			

2.2. Materials

The steel used in this study is a carbon steel (CS) (Euronorm: C35E carbon steel and US specification: SAE 1035) with its chemical composition (in wt.%) of 0.370 % C, 0.230 % Si, 0.680 % Mn, 0.016 % S, 0.077 % Cr, 0.011 % Ti, 0.059 % Ni, 0.009 % Co, 0.160 % Cu and then remainder iron (Fe). The aggressive solution of 1.0 M HCl was prepared by dilution of analytical grade 37 % HCl with distilled water.

2.3. Corrosion tests

2.3.1. Electrochemical impedance spectroscopy

The electrochemical measurements were carried out using Volta lab (Tacussel- Radiometer PGZ 100) potentiostat and controlled by Tacussel corrosion analysis software model (Voltamaster 4) at under static condition. The corrosion cell used had three electrodes. The reference electrode was a saturated calomel electrode (SCE). A platinum electrode was used as auxiliary electrode of surface area of 1 cm^2. The working electrode was carbon steel. All potentials given in this study were referred to this reference electrode. The working electrode was immersed in test solution for 30 minutes to a establish steady state open circuit potential (*E*ocp). After measuring the *E*ocp, the electrochemical measurements were performed. All electrochemical tests have been performed in aerated solutions at 303 K to reach the appropriate conditions of corrosion. The EIS experiments were conducted in the frequency range with high limit of 100 kHz and different low limit 0.1 Hz at open circuit potential, with 10 points per decade, at the rest potential, by applying 10 mV ac voltage peak-to-peak. The best semicircle can be fit through the data points in the Nyquist plot using a non-linear least square fit

so as to give the intersections with the *x*-axis. The inhibition efficiency of the inhibitor was calculated using the following equation:

$$\eta_{EIS} = \frac{R_{ct} - R_{ct}^{0}}{R_{ct}} \times 100 \quad (1)$$

where R^{0}_{ct} and R_{ct} are the charge transfer resistance values in the absence and presence of inhibitor, respectively.

2.3.2. Potentiodynamic polarization

The electrochemical behaviour of carbon steel sample in inhibited and uninhibited solution was studied by recording anodic and cathodic potentiodynamic polarization curves. Measurements were performed in the 1.0 M HCl solution containing different concentrations of the tested inhibitor by changing the electrode potential automatically from -800 mV/SCE to -200 mV/SCE at a scan rate of 1 mV s^{-1}. The linear Tafel segments of anodic and cathodic curves were extrapolated to corrosion potential to obtain corrosion current densities (i_{corr}). From the polarization curves obtained, the corrosion current (i_{corr}) was calculated by curve fitting using the equation:

$$i = i_{corr}\left[exp\left(\frac{2.3\Delta E}{\beta_a}\right) - exp\left(\frac{2.3\Delta E}{\beta_c}\right)\right] \quad (2)$$

β_a and β_c are the anodic and cathodic Tafel slopes and ΔE is $E-E_{corr}$.

The inhibition efficiency was evaluated from the measured i_{corr} values using the following relationship:

$$\eta_{PP} = \frac{i^{0}_{corr} - i_{corr}}{i^{0}_{corr}} \times 100 \quad (3)$$

where i^{0}_{corr} and i_{corr} are the corrosion current densities for carbon steel electrode in the uninhibited and inhibited solutions, respectively.

2.4. DFT calculations

E_{HOMO} (highest occupied molecular orbital energy), E_{LUMO} (lowest unoccupied molecular orbital energy) and Fukui indices calculations were performed using *DMol*^{3} module in Materials Studio version 6.0[28]. These calculations employed an *ab initio*, gradient-corrected functional (*GGA*) method with a double numeric plus polarization (DNP) basis set and a Becke One Parameter (BOP) functional. It is well-known that the phenomena of electrochemical corrosion appear in aqueous phase. *DMol*^{3} includes certain COSMO controls, which allow for the treatment of solvation effects [28,29].

2.5. Monte Carlo simulation

Experimentally, a molecular system is described by a small number of parameters, such as volume and temperature. The collection of molecular configurations that satisfy this partial knowledge is called an ensemble of configurations. Adsorption Locator module as implemented in the Materials Studio 6.0 software (Accelrys, Inc.) has been employed to compute the interaction between tested benzodiazepine derivatives and Fe (110) surface through Metropolis Monte Carlo approach[28]. A simulation box (29.78 × 29.78 × 60.13 Å) has been constructed to simulate the interaction between tested inhibitors and the Fe (110) surface. COMPASS force field was used to optimize the structures of all components of the system of interest.

3. Results and Discussion

3.1. Potentiodynamic polarization curves :

Figure 1 shows the potentiodynamic polarization curves of carbon steel in 1.0 M HCl in the absence and presence of each compound at different concentrations. These obtained curves showed that the reactions of the anodic dissolution of the metallic surface and the cathodic hydrogen evolution reaction were slowed after inhibitors addition. The slowdown of anodic and cathodic reactions is marked with rise of concentration. The tested compounds are reacted by adsorption onto the carbon steel surface, causing blockage of reaction sites. The addition of the inhibitor in hydrochloric acid causes a slight displacement of the corrosion potential (see Figure 1). According to the literature, it has been reported that if the displacement in E_{corr} in presence of inhibitor compared with E_{corr} in uninhibited solution is greater than 85 mV, the inhibitor can be considered as an anode or cathode type inhibitor, and if it is less than 85 mV, the inhibitor can be considered as mixed type [31]. From this data, the maximum displacement of E_{corr} values was 57 mV for THBD and 30 mV for CTHBD, indicating that these inhibitors act as mixed type inhibitor. The kinetic parameters values are represented in Table 2.

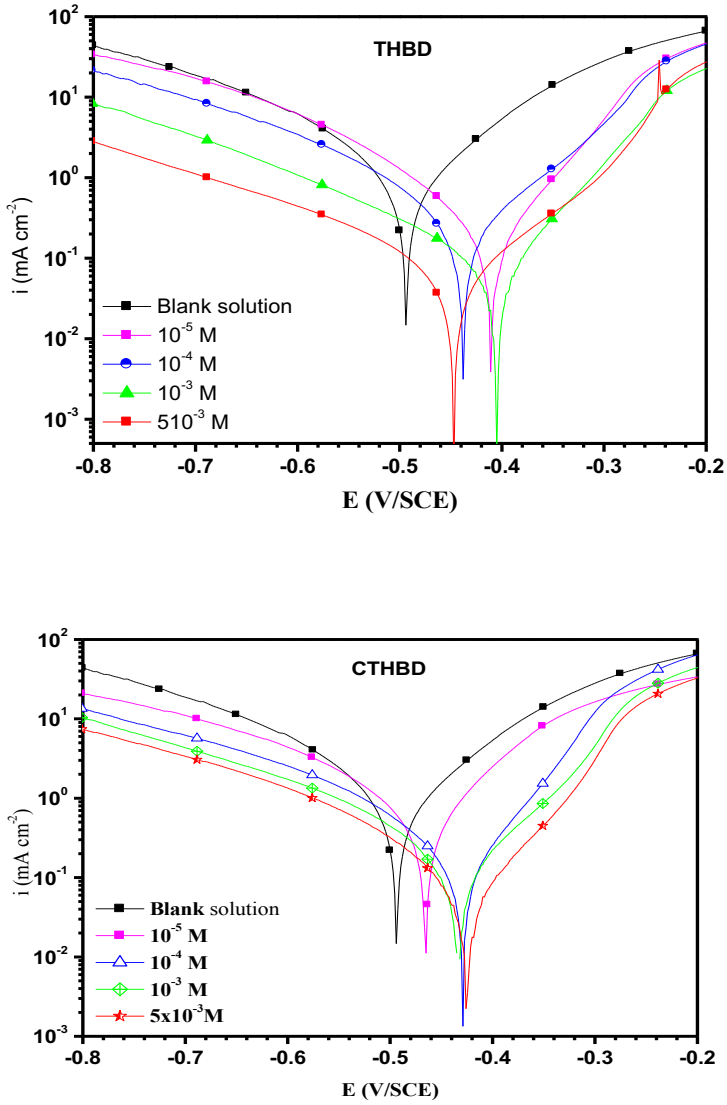

Figure 1: Potentiodynamic polarization curves of carbon steel in 1.0 M HCl without and with different concentrations of the tested inhibitors at 303 K.

Table 2. Electrochemical parameters and corresponding inhibition efficiency for carbon steel corrosion in 1.0 M HCl in the absence and the presence of different concentrations of inhibitors at 303 K.

Compounds	Conc. (M)	- E_{corr} (mV/SCE)	-β_c (mV/dec)	i_{corr} (μA/cm^2)	η_{PP} (%)
HCl	1.0	474	170	564	—
CTHBD	5×10^{-3}	452	156	45	92
	1×10^{-3}	409	150	60	87
	1×10^{-4}	441	152	183	67
	1×10^{-5}	414	154	200	64
THBD	5×10^{-3}	429	147	46	92
	1×10^{-3}	437	152	97	82
	1×10^{-4}	441	153	127	77
	1×10^{-5}	441	157	194	67

From Table 2, it is observed that the corrosion current density (i_{corr}) decreases with inhibitors addition. The presence of the inhibitors slightly changes cathodic Tafel slope (βc), which suggests that the inhibiting action is made by simple blocking of the available necessary for hydrogen evolution and lowered cathodic sites on the metal surface, which cause a decrease in the exposed area the dissolution rate with increasing inhibitor concentration [31–33]. The parallel cathodic Tafel plots obtained in Figure 1 showed that hydrogen evolution is

controlled by the activation and the presence of the inhibitor has no influence on the reduction mechanism. However, it is found that the inhibition efficiency in the presence of CTHBD and CTHBD varied from 92 to 64 % over a concentration range of 10^{-5} to 5×10^{-3} M.

3.2. Electrochemical impedance spectroscopy (EIS)

The results obtained by the PP technique are insufficient to characterize complex mechanisms. The use of EIS technique is essential. Figure 2 shows the Nyquist plots acquired at the open-circuit potential after 30 min of immersion. It is observed that the obtained Nyquist diagrams were composed by one depressed capacitive loop with one capacitive time constant. These impedances spectra were fitted to the Rs(R_{ct}/CPE) equivalent circuit presented in Figure 3. The obtained electrochemical parameters are reported in Table 3.

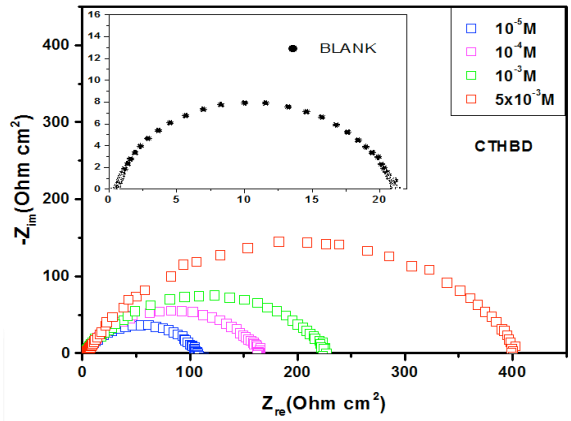

Figure 2: Nyquist plots of carbon steel in 1M HCl without and with different concentrations of inhibitors at 303K

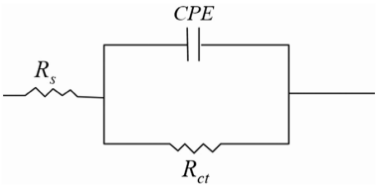

Figure 3: Equivalent electrical circuit.

Table 3: Impedance parameters recorded for carbon steel electrode in 1.0 M HCl solution in the absence and presence of different concentrations of inhibitors at 303K.

Compounds	Conc. (M)	R_{ct} (Ω cm^2)	n_{dl}	Q (Ω^{-1}cm^{-2}s^{-n})	C_{dl} (μF cm^{-2})	η_{EIS} (%)
HCl	1.0	20	0.87	1.954	85	
THBD	5×10^{-3}	517	0.74	0.8123	26	96
	1×10^{-3}	416	0.76	0.8745	27	95
	1×10^{-4}	122	0.78	0.9723	28	83
	1×10^{-5}	89	0.79	0.9978	29	77
CTHBD	5×10^{-3}	397	0.73	0.7511	20	95
	1×10^{-3}	218	0.76	0.7922	21	91
	1×10^{-4}	159	0.78	0.8011	23	87
	1×10^{-5}	106	0.79	1.145	33	81

In this circuit R_s is the solution resistance, R_{ct} denotes the charge-transfer resistance and *CPE* is constant phase element. The introduction of *CPE* into the circuit was necessitated to explain the depression of the capacitance semicircle, which corresponds to surface heterogeneity resulting from surface roughness, impurities, and adsorption of inhibitors [34–36]. The impedance of this element is frequency-dependent and can be calculated using the equation 4:

$$Z_{CPE} = \frac{1}{Q(j\omega)^n} \qquad (4)$$

where, Q is the *CPE* constant (in Ω^{-1} S^n cm^{-2}), ω is the angular frequency (in rad s^{-1}), j^2 = -1 is the imaginary number and n is a *CPE* exponent which can be used as a gauge for the heterogeneity or roughness of the

surface[36,37]. In addition, the double layer capacitances, C_{dl}, for a circuit including a *CPE* were calculated by using the following equation 5:

$$C_{dl} = \sqrt[n]{Q \times R_{ct}^{1-n}} \qquad (5)$$

It is clear from the results depicted in Table 3 that the value of R_{ct} increases whereas the value of C_{dl} decreases with the presence of inhibitors. This finding were attributed to a decrease in the local dielectric constant and/or to an increase in the thickness of the electrical double layer [39,40].

3.3. Effect of temperature

The effect of temperature on the inhibited acid–metal reaction is very complex, because many changes occur on the metal surface such as rapid etching, desorption of inhibitor and the inhibitor itself may undergo decomposition [40]. The effect of temperature on the inhibition performance of the studied inhibitors for carbon steel in 1.0 M HCl solution in the absence and presence of 5×10^{-3} M concentration at temperature ranging from 303 to 333 K was obtained by potentiodynamic polarization measurements (Figures 3-5). Their corresponding parameters are given in Table 4. The inhibition efficiencies are found to decrease with increasing of temperature solution from 303 K to 333 K. This behavior can be interpreted on the basis that the increases in temperature results in desorption of the inhibitor molecules from the carbon steel surface.

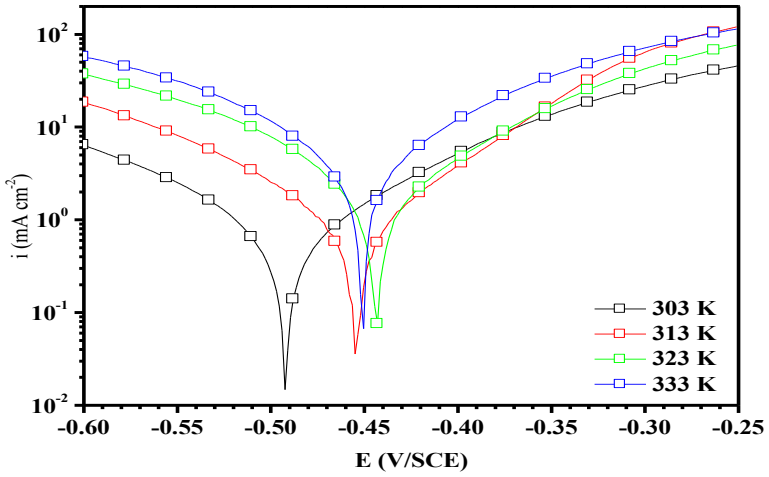

Figure 3: Potentiodynamic polarization curves for carbon steel in 1.0 M HCl at different temperatures.

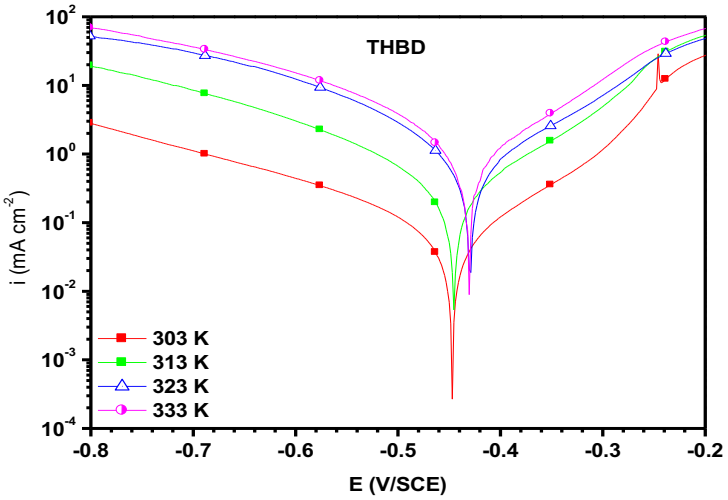

Figure 4: Potentiodynamic polarization curves for carbon steel in 1.0 M HCl in the presence of 5×10^{-3} M of THBD at different temperatures.

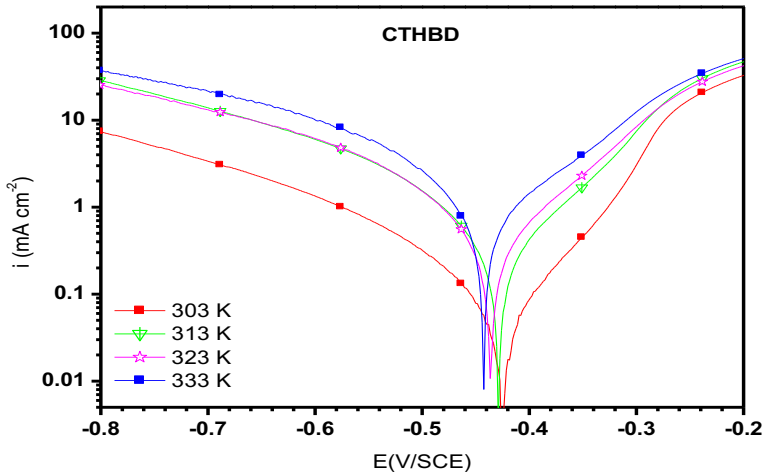

Figure 5: Potentiodynamic polarization curves for carbon steel in 1.0 M HCl in the presence of 5×10^{-3} M of CTHBD at different temperatures.

Table 4. Electrochemical parameters of carbon steel corrosion in 1.0 M HCl without and with 1×10^{-3} M of each inhibitors.

	Temperature (K)	$-E_{corr}$ (mV/SCE)	i_{corr} (mA cm^{-2})	η_{PP} (%)
Blank	303	452	564	-
	313	454	860	-
	323	443	1840	-
	333	450	2600	-
CTHBD	303	452	45	92
	313	449	150	82
	323	433	577	68
	333	435	1100	57
THBD	303	429	46	92
	313	432	147	82
	323	440	396	78
	333	446	710	72

Table 4 showed that the corrosion rate increases with increasing temperature both in uninhibited and inhibited solutions. The corrosion rate increases more rapidly with temperature in the absence of the inhibitor. These results confirm that benzodiapepine derivatives act as an efficient inhibitor for carbon steel in 1.0 M HCl in the studied range of temperature.

Consequently, the activation energy (Ea), the enthalpy of activation (ΔHa) and the entropy of activation (ΔSa) for the corrosion of carbon steel in1 M HCl in the absence and presence of 5×10^{-3} M of inhibitors are calculated using Arrhenius and transition state equations[42,43].

$$i_{corr} = k\exp\left(-\frac{E_a}{RT}\right) \qquad (6)$$

$$i_{corr} = \frac{RT}{Nh}\exp\left(\frac{\Delta S_a}{R}\right)\exp\left(\frac{\Delta H_a}{RT}\right) \qquad (7)$$

Where k is the Arrhenius pre-exponential factor, T the absolute temperature, Ea the activation corrosion energy for the corrosion process, h the Planck's constant, N the Avogadro's number, ΔS_a the entropy of activation, ΔH_a the enthalpy of activation and i_{corr} is the corrosion rate.

The plots of Ln i_{corr} versus 1/T (Figure 6) and Ln (i_{corr}/T) versus 1/T (Figure 7) show almost straight lines and all the regression coefficients are close to 1. From the slopes and intercepts of the straight lines, the values of E_a, ΔH_a and ΔS_a were calculated and listed in Table 5.

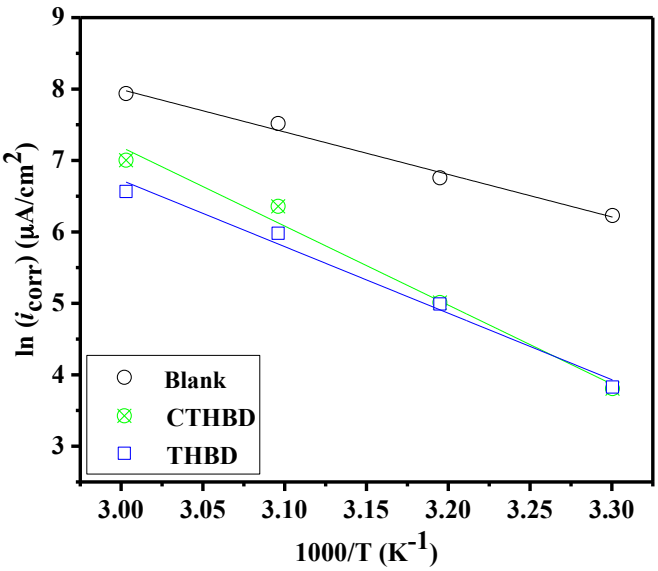

Figure 6: Arrhenius plots of Ln i_{corr} vs. 1/T for carbon steel in 1.0 M HCl in the absence and the presence of inhibitors at optimum concentration.

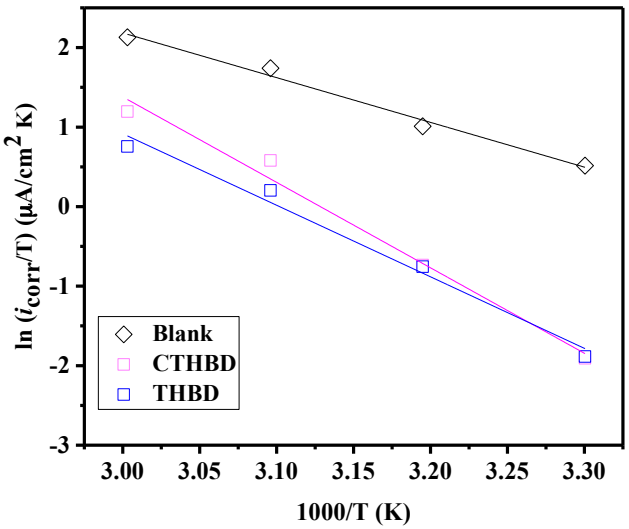

Figure 7: Relation between ln (i_{corr}/ T) and 1000/T at different temperatures.

Table 5. Activation parameters for the carbon steel dissolution in 1.0 M HCl in the absence and the presence of 5×10^{-3} M of inhibitors.

	*E*a (kJ mol^{-1})	ΔHa (kJ mol^{-1})	ΔSa (kJ mol^{-1}K^{-1})	Ea-ΔHa
Blank	49.38	46.77	-38.96	2.6
CTHBD	91.97	89.33	81.93	2.6
THBD	77.43	74.80	34.48	2.6

According to the data in Table 5, the values of E_a determined in solutions containing inhibitors are higher than that of in the absence of inhibitors, suggesting that the energy barrier of the corrosion reaction increases, meaning that the dissolution of the steel is difficult [44]. High values of E_a are generally associated with low corrosion rates while low values of E_a are associated with high corrosion rates. However, the positive sign of ΔHa reflects the endothermic nature of the carbon steel dissolution process, suggesting that the dissolution of carbon steel is slow[45] in the presence of inhibitors.

On the other hand, Table 5 shows that the values of ΔSa increase in presence of inhibitors compared to blank solution, which mean an increase in disorder takes place during the course of the transition from reactant to the activated complex during the corrosion process [46,47].

3.4. Adsorption isotherm

Because the adsorption isotherm provides some structural and thermodynamic information, it is of great importance in the corrosion field[48]. Generally, the adsorption of synthetic inhibitors is largely influenced by the nature of the testing media, the chemical structure and nature of substituents, the charge distribution, and the nature of the metal[42,43,49]. To find a suitable adsorption isotherm in the present study, several commonly used isotherms were tested, among which the Langmuir. Adsorption isotherm was found to fit well with our experimental data. The Langmuir isotherm can be represented as[50]:

$$\frac{C_{inh}}{\theta} = \frac{1}{K_{ads}} + C_{inh} \qquad (8)$$

where C(inh) is the inhibitor concentration, K_{ads} is the equilibrium constant for the adsorption–desorption process and θ is the surface coverage. The values of K_{ads} were calculated with the help of the Langmuir plot shown in Figure 8.

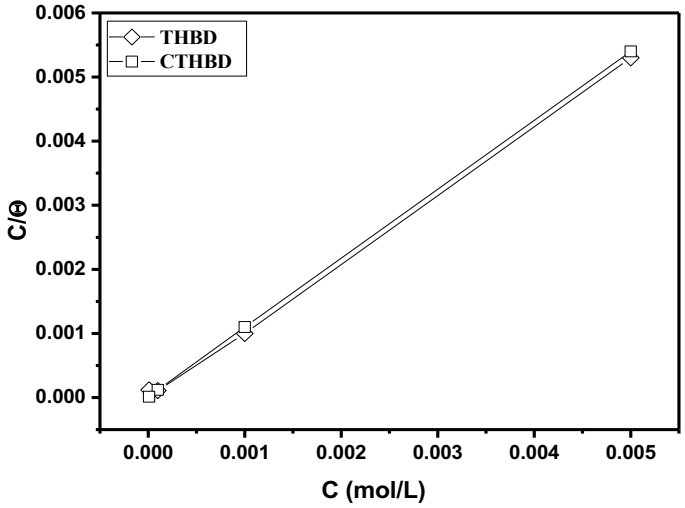

Figure 8: Langmuir adsorption isotherm plots for both inhibitors at 303K.

The K_{ads} is related to the standard free energy (ΔG^*_{ads}) of adsorption by the relation [42].

$$K_{ads} = \frac{1}{55.55}\exp\left(\frac{-\Delta G^*_{ads}}{RT}\right) \qquad (9)$$

where R is the universal gas constant, T is the absolute temperature in K, and the numerical value 55.5 represents the molar concentration of water in the acid solution. The calculated values of K_{ads} and ΔG^*_{ads} at 303 K are listed in Table 4. Generally, a high value of K_{ads} is associated with high adsorption efficiency. In our present case, the values of K_{ads} follow the order THBD < CTHBD, which is consistent with the order of the inhibition efficiency. Generally, a value of ΔG^*_{ads} of −20 kJ mol^{-1} or less negative is associated with physical adsorption resulting from electrostatic interaction between a charged inhibitor and charged metal, and a value of ΔG^*_{ads} of −40 kJ mol^{-1} or more negative is associated with chemical adsorption resulting from charged (electron) sharing between non-bonding electrons of the inhibitor and the d-orbital's of the surface Fe-atoms[39,40]. In our present study, the values of ΔG^*_{ads} were found to be between −36.65 and −38.27 kJ mol^{-1}, suggesting that the investigated benzodiazepine derivatives are adsorbed on the carbon steel surface by a physisorption mechanism[51,52].

Table 6. Adsorption parameters of studied inhibitors for mild steel corrosion in 1.0 M HCl at 303 K.

Inhibitor	Slope	K_{ads} (M^{-1})	ΔG^*_{ads} (KJ/mol)
THBD	1.05	38198	-36.65
CTHBD	1.07	87796	-38.27

3.5. Quantum chemical calculations

The quantum chemical calculation plays a vital role in selecting the best corrosion inhibitor with required structural characteristics. This theoretical approach helps to find the corrosion inhibition effectiveness which depends on the molecular structure. The calculated quantum chemical parameters related to the inhibition effect of THBD and CTHBD such as the energy of the highest occupied molecular orbital (E_{HOMO}), the energy of the lowest unoccupied molecular orbital (E_{LUMO}) and the gap energy ΔE_{gap}, were calculated and listed in Table 7. The optimized geometry, HOMO and LUMO of both inhibitors were shown in Figure 9.

Table 7. Quantum theoretical parameters for both inhibitors

Inhibitors	E_{HOMO}	E_{LUMO}	ΔE	ΔN
THBD	-3.49	-0.38	3.11	0.926
CTHBD	-4.01	-0.90	3.11	0.757

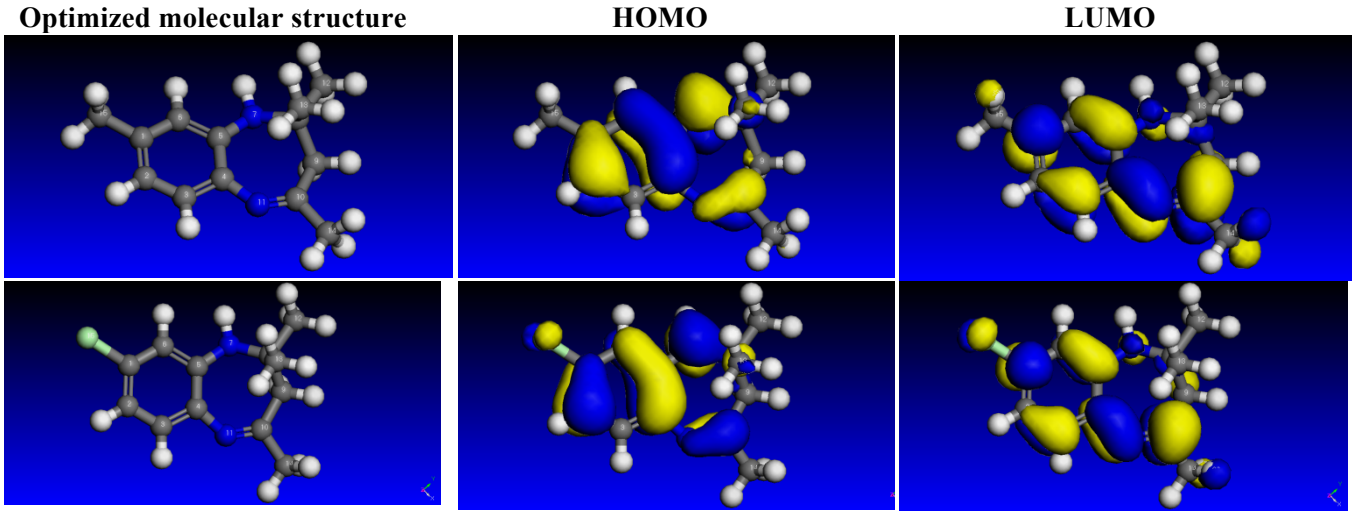

Figure 9: Optimized structure and frontier molecular orbital density distributions of studied inhibitors.

Based on the frontier molecular orbital theory, the reaction of reactants mainly occurred on the highest occupied molecular orbital (HOMO) and lowest unoccupied molecular orbital (LUMO). Therefore, it's indispensable to analyze the electron density distribution in the orbitals HOMO and LUMO of the inhibitor molecule. This distribution of HOMO and LUMO orbitals is a critical tool to predict the reactivity and consequently the ability of tested compound to adsorb on the steel surface. Higher value of E_{HOMO}, indicates that the molecule has a higher tendency to donate electrons to appropriate acceptor molecules with low energy empty molecular orbital whereas lower value of E_{LUMO}, suggesting that the molecule easily accepts electrons from the donor molecules [53]. The lower value ΔE is another important molecular parameter which favors higher inhibition ability of the inhibitor. Based on the results from Table 7, it can be inferred that the slight difference in the inhibition efficiency of both inhibitors mainly due to the little more donation ability of THBD compared to CTHBD.

However, the fraction of electrons transferred ΔN from inhibitor to carbon steel surface is also calculated. It has reported that the ΔN value measures the ability of a chemical compound to transfer its electrons to metal if $\Delta N > 0$ and vice versa if $\Delta N < 0$ [54,55]. In this study, the positive value of $\Delta N = 0.3032$ presented in Table 7, suggest the high capability of THBD to donate electrons to the carbon steel surface.

Furthermore, from Figure 9, it could be seen that both inhibitors have similar HOMO and LUMO distributions, which were all located on the entire molecular structure. This is due to the presence of nitrogen atoms together with several π-electrons on the entire molecule.

Fukui functions are used to measure the local reactivity of the inhibitors molecules and indicate their chemical reactivity for nucleophilic and electrophilic nature [56,57]. Using a scheme of finite difference approximations, this procedure condenses the values around each atomic site into a single value that characterizes the atom in the molecule. With this approximation, the condensed Fukui function becomes[58]:

$$f_k^+ = q_k(N + 1) - q_k(N) \quad \text{(For nucleophilic attack)} \qquad (10)$$

$$f_k^- = q_k(N) - q_k(N - 1) \quad \text{(For electrophilic attack)} \qquad (11)$$

Where $q_k(N+1)$, $q_k(N)$, $q_k(N-1)$ represent charge values of atom k for anion, neutral, and cation, respectively. The preferred site for nucleophilic attack is the atom in the molecule where the value of f^+ is the highest while the preferred site for electrophilic attack is the atom in the molecule where the value of f^- is the highest[58].

The values of calculated Fukui functions based on Mulliken population analysis, given in Table 8. In CTHBD and THBD, atoms C10, N11, and Cl15, and C1, C10 and N11 respectively, present the highest values of f_k^+, where are the most susceptible sites for nucleophilic attacks. On the other hand, in CTHBD, atoms C2, N7, and Cl15, in THBD, atoms C2, C4, and N7, are the susceptible sites for electrophilic attacks as they present the highest values of f_k^-. The information obtained from the Fukui condensed function entirely agrees with the analysis of the FMO.

Table 8: Values of the Fukui functions for both inhibitors.

	CTHBD		THBD	
Atom	f^+	f^-	f^+	f^-
C (1)	0.049	0.002	**0.058**	0.006
C (2)	0.020	**0.073**	0.019	**0.067**
C (3)	0.039	0.010	0.030	0.017
C (4)	0.020	0.052	0.002	**0.058**
C (5)	0.043	0.020	0.040	0.021
C (6)	0.025	0.038	0.018	0.039
N (7)	0.021	**0.101**	0.020	**0.109**
C (8)	-0.028	-0.037	-0.024	-0.040
C (9)	-0.036	-0.020	-0.032	-0.020
C (10)	**0.100**	0.048	**0.108**	0.041
N (11)	**0.070**	0.021	**0.075**	0.034
C (12)	-0.016	-0.016	-0.014	-0.019
C (13)	-0.013	-0.015	-0.017	-0.014
C (14)	-0.033	-0.014	-0.029	-0.022
Cl/C (15)	**0.120**	**0.117**	-0.023	-0.017

3.6. Monte Carlo simulation

Monte Carlo simulations were carried out to better understand the interaction between the both inhibitors and Fe (110) surface because it provides some essential parameters such as adsorption energy. In our present study the Monte Carlo simulation calculation was used to find the lowest energy for the whole system. Figure 10 represents the most stable low energy configuration for the adsorption of inhibitors on Fe (110) surface obtained through the Monte Carlo simulations.

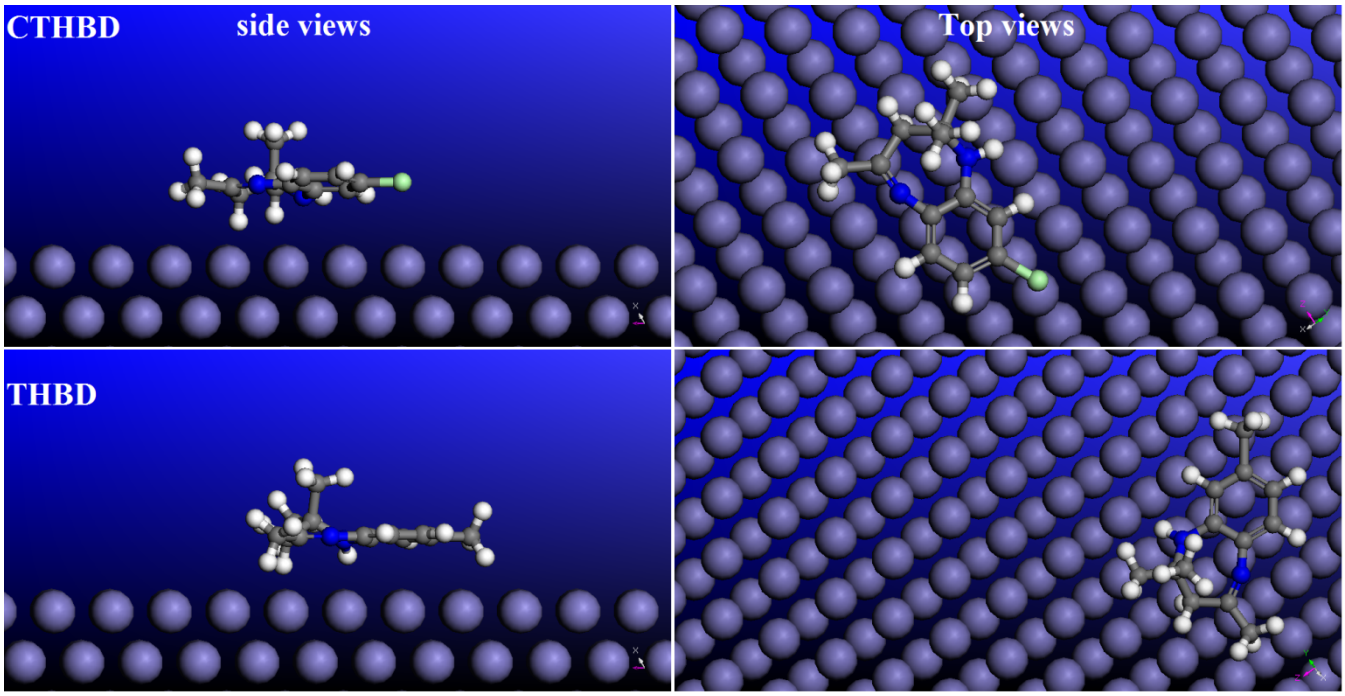

Figure 10: The most stable low energy configuration for the adsorption of the inhibitors on Fe (1 1 0) surface obtained through the Monte Carlo simulation.

It is by and large recognized that the essential phenomenon of corrosion inhibition of carbon steel is by adsorption. So the adsorption energy can furnish us with immediate information about the efficiency of

inhibitors. The results depicted in Table 9 show that the both compounds associated with high negative values of adsorption energy resulting in the strong interactions between metal and inhibitor molecules [60]. By inspection of the Figure 10, it could be observed that the benzodiazepine derivatives adsorb nearly to Fe (110) surface, were a chemical interactions can possibly occur through reactive sites in the molecule as interpreted in experimental and theoretical study[61].

Table 9. Outputs and descriptors calculated by the Monte Carlo simulation for the lowest adsorption. configurations of inhibitors on Fe (110) surface (in kcal/mol).

System	Total energy	Adsorption energy	Rigid adsorption energy	Deformation energy	dEad/dNi inhibitor
Fe (110)/**THBD**	400.66	-300.50	-280.0	-20.50	-300.50
Fe (110)/**CTHBD**	546.05	-290.40	-278.3	-12.10	-290.40

Conclusion

In this paper, the corrosion inhibition of carbon steel in 1.0 M HCl solutions by two benzodiazepine derivatives was studied using electrochemical techniques, quantum chemical calculations and Monte Carlo simulations. Both compounds are good corrosion inhibitors for carbon steel in acid solution. The inhibition efficiency of these compounds depends on its concentration and temperatures. Polarization curves indicated that both compounds act as mixed type inhibitors. EIS plots indicated that R_{ct} values increase and C_{dl} values decrease with increasing inhibitor concentration. The adsorption of tested inhibitors on carbon steel surface follows Langmuir adsorption isotherm. The quantum chemical parameters are obtained and discussed in view of experimental results. Both experimental, quantum chemical and Monte Carlo simulations results showed that the inhibition efficiency of both inhibitors is affected by the heteroatoms and π-system presented in our compounds.

References

1. H. Jafari, I.Danaee , H.Eskandari,M. RashvandAvei ,*J. Mater .Sci. Technol.30* (2014) 239.
2. M. Rbaa, M. Galai, M. EL Faydy, Y. El Kacimi, M. Ebn Touhami, A. Zarrouk, B. Lakhrissi, *J. Mater . Environ .Sci*. 8 (10) (2017) 3529.
3. M. Larouj,H.Lgaz, H.Serrar, H.Zarrok, H.Bourazmi, A.Zarrouk, A.Elmidaoui, A.Guenbour, S.Boukhris, H. Oudda , *J.Mater .Environ .Sci.6* (2015) 3251.
4. M. Belayachi, H. Serrar, A. El Assyry, H. Oudda, S. Boukhris, M. Ebn Touhami, A. Zarrouk, B. Hammouti, Eno E. Ebenso, A. El Midaoui, Int. J. Electrochem. Sci. 10 (2015) 3038.
5. RN. Singh, A. Kumar, RK. Tiwari, P. Rawat , *Spectrochim .Acta .A .Mol. Biomol .Spectrosc.*112 (2013)182–190
6. A. Ghazoui, R. Saddik, N. Benchat, B. Hammouti, M. Guenbour, A. Zarrouk, M. Ramdani, Der Pharm. Chem. 4 (2012) 352.
7. H. Zarrok, R. Saddik, H. Oudda, B. Hammouti, A. El Midaoui, A. Zarrouk, N. Benchat, M. Ebn Touhami, Der Pharm. Chem. 3 (2011) 272.
8. T. Laabaissi, H.Lgaz,H.Oudda, F.Benhiba, H.Zarrok, A.Zarrouk, A.El Midaoui, B.Lakhrissi, R.Touir , *J. Mater .Environ Sci*.8(2017) 1054.
9. A. Zarrouk, B. Hammouti, R. Touzani, S.S. Al-Deyab, M. Zertoubi, A. Dafali, S. Elkadiri, Int. J. Electrochem. Sci. 6 (2011) 4939.
10. M. Rbaa, M. Galai, Y. El Kacimi, M. Ouakki, R. Touir, *Portugaliae Electrochimica Acta* 35(6) (2017) 323.
11. A. Zarrouk, B. Hammouti, A. Dafali, H. Zarrok, Der Pharm. Chem. 3 (2011) 266.
12. A. Ghazoui, A. Zarrouk, N. Bencaht, R. Salghi, M. Assouag, M. El Hezzat, A. Guenbour, B. Hammouti, J. Chem. Pharm. Res. 6 (2014) 704.
13. H. Zarrok, A. Zarrouk, R. Salghi, H. Oudda, B. Hammouti, M. Assouag, M. Taleb, M. Ebn Touhami, M. Bouachrine, S. Boukhris, J. Chem. Pharm. Res. 4 (2012) 5056.
14. H. Zarrok, A. Zarrouk, R. Salghi, M. Assouag, B. Hammouti, H. Oudda, S. Boukhris, S.S. Al Deyab, I. Warad, Der Pharm. Lett. 5 (2013) 43
15. M. Rbaa, M. Galai, M. El Faydy, Y. El Kacimi, M. Ebn Touhami, A. Zarrouk, B. Lakhrissi, *Anal. Bioanal. Electrochem* .9(7)(2017) 904.
16. M. Belayachi, H. Serrar, H. Zarrok, A. El Assyry, A. Zarrouk, H. Oudda, S. Boukhris, B. Hammouti, E.E. Ebenso, A. Geunbour, Int. J. Electrochem. Sci. 10 (2015) 3010.
17. A. Zarrouk, H. Zarrok, R. Salghi, R. Touir, B. Hammouti, N. Benchat, L.L. Afrine, H. Hannache, M. El Hezzat, M. Bouachrine, J. Chem. Pharm. Res. 5 (2013) 1482.

18. H. Zarrok, A. Zarrouk, R. Salghi, M. Ebn Touhami, H. Oudda, B. Hammouti, R. Touir, F. Bentiss, S.S. AlDeyab, Int. J. Electrochem. Sci. 8 (2013) 6014.
19. D. Ben Hmamou, M.R. Aouad, R. Salghi, A. Zarrouk, M. Assouag, O. Benali, M. Messali, H. Zarrok, B. Hammouti, J. Chem. Pharm. Res. 4 (2012) 34984.
20. M. El Faydy, M. Galai, R. Touir, A. El Assyry, M. Ebn Touhami, B. Benali, B. Lakhrissi, A. Zarrouk, J. Mater. Environ. Sci. 7 (4) (2016) 1406.
21. H. Lgaz, R.Salghi, M.Larouj,M. Elfaydy, S.Jodeh,Z. Rouifi,B. Lakhrissi,H. Oudda ,*J. Mater. Environ .Sci*. 7 (2016) 4471.
22. M. Larouj, H.Lgaz, S.Rachid,H. Oudda , S.Jodeh, A.Chetouani,*Moroc. J .Chem*..**4** (2016) 425.
23. M. Elfaydy, H.Lgaz, R.Salghi, M.Larouj, S.Jodeh, M.Rbaa, H.Oudda, K.Toumiat, B.Lakhrissi,*J. Mater. Environ .Sci.7* (2016) 3193.
24. H. Lgaz, M. Saadouni, R.Salghi,S. Jodeh, M.Elfaydy,B. Lakhrissi, S.Boukhris,H. Oudda , *Pharm. Lett*. 8 (2016) 158.
25. Y. El Aoufir, H.Lgaz, K.Toumiat, R.Salghi, S.Jodeh, M.Zougagh,A. Guenbour, H.Oudda,*Res. J. Pharm. Biol .Chem. Sci*.7(2016) 1219.
26. IB. Obot , DD.Macdonald, ZM.Gasem , *Corros .Sci*.99(2015) **9**1.
27 Shi, R. X, Liu, Y. K, & Xu, Z. Y. *J. of Zhejiang University-Science B*, *11*(2), (2010),102
28. Materials Studio, *Revision 6.0*,Accelrys .Inc. San .Diego. USA (2013).
29. B. Delley,*J.Chem .Phys*.92(1990) 508.
30. Delley B. *J .Chem .Phys* .113(2000) 7756.
31. L. Afia, R.Salghi, A.Zarrouk, H.Zarrok, EH.Bazzi,B.Hammouti, M.Zougagh , *Trans Indian Inst.Met* .66(2013) 43.
32. N. Yilmaz,A. Fitoz, Ergun ÿmit, KC.Emregül ,*Corros Sci* .111(2016)110.
33. R. Yıldız,*Corros .Sci.90* (2015) 544.
34. M. Yadav, R. Sinha, S. Kumar, T. Sarkar, *RSC .Adv.5* (2015) 70832.
35. DK. Yadav, B.Maiti, M.Quraishi,*Corros .Sci* .52(2010) 3586.
36. C. Verma, MA.Quraishi, LO.Olasunkanmi, EE.Ebenso,*RSC. Adv* .5(2015) 85417.
37. MA. Amin, M.Ahmed, H.Arida, T.Arslan, M.Saracoglu, F.Kandemirli ,*Corros. Sci* .53(2011) 540.
38. Amin MA, El-Rehim SA, El-Sherbini E, Bayoumi RS. *Int .J .Electrochem .Sci* .3(2008) 199.
39. C. Verma, MA.Quraishi, A.Singh,*J. Mol. Liq212.* (2015) 804.
40. Singh DK, Kumar S, Udayabhanu G, John RP. *J. Mol .Liq* .216(2016) 738.
41. M. Lebrini, F.Bentiss, H.Vezin, M.Lagrenée, *Corros .Sci* .48(2006) 1279.
42. C. Verma, EE.Ebenso, I.Bahadur, IB.Obot, MA.Quraishi, *J. Mol .Liq .212* (2015) 209.
43. M. Yadav, L.Gope, N.Kumari, P.Yadav,*J. Mol .Liq.216* (2016) 78.
44. GK. Gomma, MH.Wahdan,*Mater .Chem .Phys* .39(1995) 209.
45. H. Gerengi, K.Darowicki, G.Bereket, P.Slepski,*Corros. Sci.51* (2009)2573.
46. AK. Singh, M.Quraishi, *Corros. Sci* .53(2011) 1288.
47. E. Khamis, A.Hosny, S.Elhadary,*Afinidad.52* (1995) 95.
48. k. Anupama, k.Ramya, A.Joseph, *J. Mol .Liq* .2016(2016) 146.
49. M. Yadav, RR.Sinha , TK.Sarkar, I.Bahadur, EE.Ebenso,*J .Mol .Liq.212* (2015) 686.
50. M. Yadav, RR.Sinha, S.Kumar, I.Bahadur, EE.Ebenso,*J .Mol .Liq.208* (2015) 322.
51. S. Kaya, B.Tüzün, Kaya .C,I.B. Obot , J. Taiwan Inst. Chem. Eng.58 (2016) 528.
52. H. Lgaz,K. Subrahmanya Bhat, R.Salghi, Shubhalaxmi, S.Jodeh, M.Algarra, B.Hammouti, IH.Ali, A. Essamri , *J .Mol .Liq.238* (2017) 71.
53. S. Xia, M.Qiu, L.Yu, F.Liu,H. Zhao ,*Corros .Sci.50* (2008) 2021.
54. N. Kovačević, A.Kokalj,*Corros. Sci.53* (2011) 909.
55. A. Kokalj,*Electrochimica .Acta* 56 (2010) 745.
56. J. Saranya, P.Sounthari, K.Parameswari, S.Chitra,*Measurement* .77 (2016) 175.
57. SK. Saha, P. Ghosh, A. Hens, NC. Murmu, P. Banerjee ,*Phys. E .Low-Dimens Syst Nanostructures*. 66 (2015) 332.
58. H.Lgaz, R. Salghi, and S. Jodeh. *Int. J. Corros. Scale .Inhib* .5.4 (2016) 347.
59. N.Karakus, K.Sayin, *J .Taiwan .Inst .Chem. Eng* .48 (2015) 95.
60. K. F. Khaled, MA. Amin, *Corros. Sci*. 51 (2009) 2098.
61. Z. Zhang , N.Tian, X.Huang ,W. Shang , Wu .L. *RSC .Adv* .6 (2016) 22250.